2024 IEEE International Conference on Artificial Intelligence in Engineering and Technology (IICAIET)

Precoding-assisted FDMA Transmission Scheme: a CP- available FBMC Technique

Ying Wang [1,*], Jianhong Xiang [1,2], Linyu Wang [1,3]

[1] College of Info. & Comm. Engineering
Harbin Engineering University
Harbin, China
Email: wangyingstu@163.com [*], xiangjianhong@hrbeu.edu.cn [2], wanglinyu@hrbeu.edu.cn [3],

2024 IEEE International Conference on Artificial Intelligence in Engineering and Technology (IICAIET) | 979-8-3503-8969-2/24/$31.00 ©2024 IEEE | DOI: 10.1109/IICAIET62352.2024.10729925

***Abstract*—Offset Quadrature Amplitude Modulation-based Filter Bank Multi-Carrier (FBMC) system provides superior spectral properties over Orthogonal Frequency Division Multiplexing. However, seriously affected by imaginary interference, its performances are hampered in many areas. In this paper, we propose a Precoding-Assisted Frequency Division Multiple Access (PA-FDMA) modulation scheme. By spreading FBMC symbols into the frequency domain and transmitting them with a precoding matrix, the impact of imaginary interference can be eliminated. Specifically, we first generate the coding presolution matrix with nonuniform Fast Fourier Transform and pick the best columns by introducing auxiliary factors. Secondly, according to the column indexes, we obtain the precoding matrix for one symbol and impose scaling factors to ensure that the power is approximately constant throughout the transmission time. Finally, we map the precoding matrix of one symbol to multiple symbols and transmit multiple data frames, thus achieving frequency-division multiple access. Additionally, observing the interference between adjacent frames, we mitigate them by adding frequency Cyclic Prefixes (CP) and evaluating them with signal-to-interference ratio. Note that PA-FDMA can be considered a CP-available FBMC technique because the underlying strategy is FBMC. Simulation results show that the proposed scheme has better performance compared to Single Carrier Frequency Division Multiple Access (SC-FDMA) etc.**

***Index Terms*—PA-FDMA, SC-FDMA, FBMC, Nonuniform Fast Fourier Transform**

I. Introduction

Future wireless systems should support robust transmission over highly fast time-varying channels [1]. However, because of high synchronization error sensitivity, Orthogonal Frequency Division Multiplexing (OFDM) hardly meets the requirements [2]. Filter Bank Multi-Carrier (FBMC) based on Offset Quadrature Amplitude Modulation (OQAM) becomes a possible candidate. Because it features high bandwidth efficiency, low synchronization error sensitivity, and more robustness to time-varying channels [3]–[5]. Although the 3rd Generation Partnership Project (3GPP) failed to select FBMC as 5G's new waveform, the technique is still a key focus of R&D for future wireless systems [6]. However, restricted by the Balian-Low theorem [7], the orthogonality of FBMC holds only in the real domain. This leads to inherent imaginary interference in the system, then, channel estimation and multiple-input-multiple-output implementations are hampered [8], [9]. R. Zakaria et al [10] utilized the Fast Fourier Transform (FFT) to spread the symbols into the time (or frequency) domain, thus eliminating imaginary interference. However, adopting FFT spreading not only increases the system complexity but also the Peak-to-Average Power Ratio (PAPR) becomes worse. R. Nissel et al [11], [12] concluded that the Hadamard matrix-based spreading scheme is superior to FFT spreading. The reason is that the complex orthogonality of the FBMC is perfectly restored within the spreading block. However, the Hadamard matrix-based spreading scheme has poor PAPR, and the Bit Error Rate (BER) performance is not desirable enough. For the aim of reducing PAPR, R. Nissel et al [13] proposed Pruned DFT-Spread FBMC. The scheme follows the idea of Single Carrier Frequency Division Multiple Access (SC-FDMA). However, Pruned DFT-Spread FBMC has interference residues. On the other hand, T. Ihalainen and D. Na et al [14], [15] similarly realized the combination of DFT and FBMC. However, both have high PAPR. We refer to many techniques applied to reduce PAPR in OFDM, e.g., selective mapping [16] or partial transmit sequences [17]. All these techniques can be adopted directly for FBMC but require high computational complexity. Fortunately, SC-FDMA [18], [19], which is used for Long Term Evolution (LTE), not only has low complexity but also can be easily implemented. The principle is precoding OFDM symbols with DFT. Our work draws on the SC-FDMA ideas and provides the following novel contributions:

- Instead of DFT, we employ Nonuniform Fast Fourier Transform (UNFFT) to spread the FBMC symbols. UNFFT not only supports both uniform and non-uniform sampled data but also enables to improve the accuracy and operation speed. This assists in maintaining system performance and reducing time complexity..
- Unlike SC-FDMA, we pick part of the coding pre-

*Corresponding Author: Ying Wang.
This work is supported in part by Fundamental Research Funds for the Central Universities, China [3072022CF0801], Collaborative Research on Key Technologies for Maritime Search and Positioning Based on the BeiDou Navigation System, China [2018YFE0206500], and Sichuan Provincial Key Laboratory of Agile Intelligent Computing Project Fund.

979-8-3503-8969-2/24/$31.00 ©2024 IEEE

solution matrix columns with specific criteria, rather than all. This corresponds to a rational zeroing the base pulse, which is beneficial to ensure lower Out-of-Band (OOB) emission.

- For chosen precoding matrix, we introduce a scaling factor, which ensures that the transmitted power is approximately constant throughout the transmission time. This is beneficial to ensure a better PAPR.
- We provide the FBMC with the usage of the frequency Cyclic Prefix (CP). In the special case, we can introduce the frequency CP to improve the Signal-to-Interference Ratio (SIR). However, when the transmission medium is dominated by noise (i.e., SNR < SIR), adding CPs no longer enhances the reliability of the system. Thus, CP is not required when the transmission environment is dominated by noise.

Notation: Bold uppercase and lowercase letters denote matrix and vector, respectively. $\mathrm{diag}\{\cdot\}$ denotes the diagonal elements of a matrix or generating a diagonal matrix from a vector. $\mathrm{Tr}\{\cdot\}$ denotes the trace of a matrix and $\mathrm{E}(\cdot)$ the expectation. $\otimes$ denotes the Kronecker product. $(\cdot)^*$, $(\cdot)^T$ and $(\cdot)^H$ denote conjugation, transposition, and conjugate transposition, respectively. The imaginary unit is denoted as $\mathrm{j}=\sqrt{-1}$. $\mathbf{I}_n$ denotes the $n \times n$ unit matrix. $\mathbb{R}$ denotes the real domain and $\mathbb{C}$ the complex domain.

II. System Model

In FBMC, real-valued OQAM symbols are usually mapped in rectangular time-frequency grids for transmission. Interference is circumvented between symbols by a phase shift factor and real orthogonality holds. Assuming that the transmitted signal $s(t)$ consists of L subcarriers and K time symbols, we can express it as

$$s(t)=\sum_{k=1}^{K}\sum_{l=1}^{L}x_{l,k}\underbrace{p(t-kT)\mathrm{e}^{\mathrm{j}2\pi lF(t-kT)}\mathrm{e}^{\mathrm{j}\pi(l+k)/2}}_{g_{l,k}(t)} \tag{1}$$

Where $x_{l,k}$ denotes the real-valued OQAM symbol. l denotes the subcarrier position and k the time position. F denotes the frequency spacing and T the time spacing. $p(t)$ denotes the prototype filter and $\mathrm{e}^{\mathrm{j}\pi(l+k)/2}$ the phase shift factor. $g_{l,k}(t)=p(t-kT)\mathrm{e}^{\mathrm{j}2\pi lF(t-kT)}\mathrm{e}^{\mathrm{j}\pi(l+k)/2}$ denotes the base pulse. In this paper, we employ the PHYDYAS prototype filter [20]. At the receiver, the received signal $r(t)$ is denoted as

$$r(t)=\int_{\mathbb{R}}s(\tau)\,h(t-\tau)\,\mathrm{d}\tau+\mathrm{n}(t) \tag{2}$$

Where $h(t)$ denotes channel impulse response. $\mathrm{n}(t)$ denotes noise. The received symbol $y_{l,k}$ can be obtained by projecting $r(t)$ onto the base pulse, denoted as

$$y_{l,k}=\int_{\mathbb{R}}r(t)g_{l,k}^*(t)\mathrm{d}t \tag{3}$$

The above continuous time model provides an intuitive understanding of the system. To simplify the analysis, we employ N-point sampling of the base pulse with rate f_s, and represent the samples with vector $\mathbf{g}_{l,k}\in\mathbb{C}^{N\times 1}$. Then, we integrate all the vectors into the transfer matrix $\mathbf{G}=[\mathbf{g}_{1,1},\cdots,\mathbf{g}_{L,K}]\in\mathbb{C}^{N\times LK}$. A wireless channel can be modeled with a time-varying convolution matrix $\mathbf{H}\in\mathbb{C}^{N\times N}$ [21]. Thereby, the global system model can be denoted as

$$\mathbf{y}=\mathbf{G}^H\mathbf{H}\mathbf{G}\mathbf{x}+\mathbf{n} \tag{4}$$

Where $\mathbf{x}=[x_{1,1},\cdots,x_{L,K}]^T\in\mathbb{R}^{LK\times 1}$ denotes the transmitted symbol and $\mathbf{y}=[y_{1,1},\cdots,y_{L,K}]^T\in\mathbb{C}^{LK\times 1}$ the received symbol. $\mathbf{n}\sim\mathcal{CN}(\mathbf{0},P_{\mathrm{n}}\mathbf{G}^H)$ denotes complex Gaussian noise.

If the channel is approximately frequency-flat within a certain frequency spacing, then FDMA can be implemented, only a precoding matrix needs to be introduced. To ensure no loss in spectral efficiency and compatibility with SC-FDMA, the system must be able to transmit complex-valued symbols $\tilde{\mathbf{x}}=[x_{1,1},\cdots,x_{L/2\ ,K}]^T\in\mathbb{R}^{LK/2\ \times 1}$. Our approach involves replacing the traditional complex-to-real mapping in FBMC with precoding. This necessitates that the dimension of the precoding matrix be $\boldsymbol{\mathcal{P}}\in\mathbb{C}^{LK\times LK/2}$. Thereby, the transmission model of PA-FDMA can be represented as

$$\tilde{\mathbf{y}}=\boldsymbol{\mathcal{P}}^H\mathbf{G}^H\mathbf{H}\mathbf{G}\boldsymbol{\mathcal{P}}\tilde{\mathbf{x}}+\boldsymbol{\mathcal{P}}^H\mathbf{n} \tag{5}$$

Where $\tilde{\mathbf{y}}=[y_{1,1},\cdots,y_{L/2\ ,K}]^T\in\mathbb{R}^{LK/2\ \times 1}$ denotes the received complex symbol. To mitigate interference between precoding subframes, we can employ frequency CP. Note that frequency CP incurs a reduction in spectral efficiency since the subcarriers allocated to CP cannot transmit useful signals. Although precoding introduces additional complexity, the added complexity is relatively minor compared to the system's inherent complexity. The complexity of our scheme is about twice that of SC-FDMA, since the underlying strategy of PA-FDMA is FBMC.

III. Mathematical Detail

In Section III-A, we present the fundamental conceptual origin and provide the procedure for generating the precoding matrix. In Section III-B, we analyze the interference scenario in PA-FDMA and provide a rigorous mathematical description.

A. Precoding matrix

All the base pulses of the multicarrier system are superimposed through a set of random weights (data symbols). Thereby, according to the Central Limit Theorem, the signal follows a Gaussian distribution. This leads to both conventional FBMC and OFDM exhibiting higher PAPR. In SC-FDMA [18], the authors applied a DFT operation to the base pulses of conventional OFDM, thus emulating single-carrier transmission. In particular, the duration of the base pulses becomes shorter, and 1-2 base pulses determine the signal for a time sample. Thus, if the data symbols are not Gaussian distributed, then the PAPR is lower than OFDM. The concept of precoding in this paper is inspired by SC-FDMA, as the data symbols in FBMC are selected from a fixed alphabet, such as Quadrature Amplitude Modulation (QAM) or Pulse Amplitude Modulation (PAM). On the other hand, both SC-FDMA and OFDM have poor OOB emissions. The concept of zero-tail DFT-spread-OFDM [22], [23] involves zeroing the edge base pulses to reduce OOB emission. We adopt the same idea, only removing the $L/2$ base pulse. Compared to DFT-spread-OFDM, our scheme incurs no overhead. The reason is that the underlying strategy ensures a twofold reduction in the time spacing. This also precisely satisfies the dimensional requirements of the precoding matrix.

Let us now discuss the process of generating the precoding matrix. As described above, we need to remove $L/2$ base pulses, which correspond to zeroing half columns of the precoding matrix. Simply picking half the columns of the precoding matrix is not viable because the total transmit power cannot be guaranteed to be approximately constant over the transmission time. To address this issue, we introduce auxiliary factor α and scaling factor β, and employ the NUFFT [24], [25] to generate the precoding matrix. The detailed precoding matrix generation process is provided below:

Step 1: Generate coding pre-solution matrix.

$$\boldsymbol{\mathcal{P}}_{\text{pre.}} = \frac{1}{\sqrt{L - L_{CP}}} nufft\left(\mathbf{I}_{L-L_{CP}}\right) \tag{6}$$

Step 2: Obtain the optimal column index vector based on the auxiliary factor.

$$\alpha = \left|\text{diag}\left(\boldsymbol{\mathcal{P}}_{\text{pre.}}^{H}\mathbf{C}_{RX}^{H}\mathbf{G}_{k}^{H}\mathbf{G}_{k}\mathbf{C}_{TX}\boldsymbol{\mathcal{P}}_{\text{pre.}}\right)\right| \tag{7}$$

$$\tilde{\alpha} = sort\left(\alpha, 'descend'\right) \tag{8}$$

$$\widehat{\alpha} = \left[\tilde{\alpha}\right]_{(L-L_{CP})/2} \tag{9}$$

If $\alpha > \widehat{\alpha}$, then save the indexed value of α into $\boldsymbol{\vartheta} \in \mathbb{R}^{1\times(L-L_{CP})/2}$, else discard the α indexed value.

Step 3: Obtain the precoding matrix of one symbol and impose the scaling factor.

$$\boldsymbol{\mathcal{P}}_{k} = \left[\boldsymbol{\mathcal{P}}_{\text{pro.}}\right]_{:,\boldsymbol{\vartheta}} \tag{10}$$

$$\beta = \sqrt{2/\alpha_{\boldsymbol{\vartheta}}} \tag{11}$$

$$\boldsymbol{\mathcal{P}}_{k} = \boldsymbol{\mathcal{P}}_{k}\text{diag}\left(\beta\right) \tag{12}$$

Step 4: Obtain the precoding matrix of all symbols.

$$\boldsymbol{\mathcal{P}} = \boldsymbol{\mathcal{P}}_{k} \otimes \mathbf{I}_{K} \in \mathbb{C}^{(L-L_{CP})K\times(L-L_{CP})K/2} \tag{13}$$

In the process, $nufft(\cdot)$ denotes Non-Uniform Fast Fourier Transform operation, which supports both uniform and non-uniform sampled data. Moreover, it improves accuracy and computing speed. $\mathbf{C}_{RX} \in \mathbb{C}^{L\times(L-L_{CP})}$ and $\mathbf{C}_{TX} \in \mathbb{C}^{L\times(L-L_{CP})}$ denote the received and transmitted frequency CP matrices, respectively, defined as

$$\mathbf{C}_{RX} = \left[\mathbf{0}_{L_{CP}/2\ ,(L-L_{CP})}, \mathbf{I}_{L-L_{CP}}, \mathbf{0}_{L_{CP}/2\ ,(L-L_{CP})}\right]^{T} \tag{14}$$

$$\mathbf{C}_{TX} = \begin{bmatrix} \mathbf{0}_{L_{CP}/2\ ,(L-(L_{CP}/2\ +1))}, \mathbf{I}_{L_{CP}/2} \\ \mathbf{I}_{L-L_{CP}} \\ \mathbf{I}_{L_{CP}/2}\ , \mathbf{0}_{L_{CP}/2\ ,(L-(L_{CP}/2\ +1))} \end{bmatrix} \tag{15}$$

The aim of adding frequency CP is to mitigate interference, which will provide more clarity when analyzing system interference. Note that the CP length must be a multiple of two. The reason is that the CP of each subframe exists in pairs at the start and the end.

B. Interference analysis

The precoding matrix shortens the duration of base pulses, resulting in an approximate time-flat characteristic for each pulse. This enables the FBMC to exhibit orthogonal transmission, as imaginary interference is eliminated. When $L \to \infty$, the pulse duration approaches zero. So, the larger the subcarrier number L, the cleaner the interference is eliminated. However, in practice, L is always finite and interference is difficult to eliminate completely. Thus, we periodically expand the symbols in the frequency domain, i.e., CP. Interference cancellation can be measured by SIR. For one symbol, the power P_{S-k} can be expressed as

$$P_{S-k} = \text{Tr}\left(\left|\boldsymbol{\mathcal{P}}_{k}^{H}\mathbf{C}_{RX}^{H}\mathbf{G}_{k}^{H}\mathbf{G}_{k}\mathbf{C}_{TX}\boldsymbol{\mathcal{P}}_{k}\right|^{2}\right) \tag{16}$$

Thereby, the SIR of one symbol can be expressed as

$$\text{SIR}_{k} = \frac{P_{S-k}}{\left\|\boldsymbol{\mathcal{P}}_{k}^{H}\mathbf{C}_{RX}^{H}\mathbf{G}_{k}^{H}\mathbf{G}_{k}\mathbf{C}_{TX}\boldsymbol{\mathcal{P}}_{k}\right\|_{F}^{2} - P_{S-k}} \tag{17}$$

Where $||\cdot||_{F}$ denotes the Frobenius norm. When we transmit multiple subframes, interference may occur between subframes. Equation (17) ignores frame interference, but now we take it into consideration. Considering more FBMC symbols, we can compute the CP matrix of the global system, denoted as

$$\widehat{\mathbf{C}}_{TX} = \mathbf{I}_{K} \otimes \mathbf{C}_{TX} \tag{18}$$

$$\widehat{\mathbf{C}}_{RX} = \mathbf{I}_{K} \otimes \mathbf{C}_{RX} \tag{19}$$

Thereby, the power P_{S} of the signal can be expressed as

$$P_{S} = \text{Tr}\left(\left|\boldsymbol{\mathcal{P}}^{H}\widehat{\mathbf{C}}_{RX}^{H}\mathbf{G}^{H}\mathbf{G}\widehat{\mathbf{C}}_{TX}\boldsymbol{\mathcal{P}}\right|^{2}\right) \tag{20}$$

The global system SIR can be written as

$$\text{SIR} = \frac{P_{S}}{\left\|\boldsymbol{\mathcal{P}}^{H}\widehat{\mathbf{C}}_{RX}^{H}\mathbf{G}^{H}\mathbf{G}\widehat{\mathbf{C}}_{TX}\boldsymbol{\mathcal{P}}\right\|_{F}^{2} - P_{S}} \tag{21}$$

Note that although (17) and (21) are structurally the same, they each contain different interference (imaginary interference and interframe interference). The reason for this distinction is that each symbol experiences different interference at different moments. To explicitly evaluate the SIR case, we calculate the maximum, mean and minimum values of the SIR at the same time position. Fig. 1 shows the variation of SIR with the subcarrier number L. Adding a set of CPs (i.e., $L_{CP} = 2$) can boost the SIR by about 14dB. When the SIR is high enough, we can obtain better BER performance without CP.

IV. Numerical Results

In this section, we perform numerical analysis. In Section IV-A, we calculate PAPR for different systems and provide PAPR performance curves. In Section IV-B, we simulate the transmission performance of the system over different channels and provide BER results.

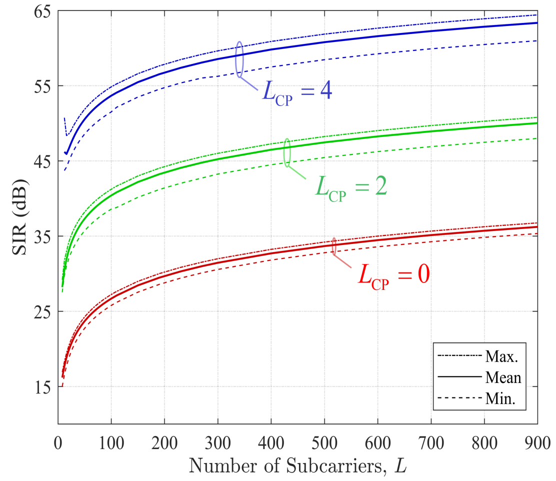

Fig. 1. Variation of SIR with the subcarrier number. At high subcarrier numbers, the SIR is high enough that we can ignore the interference. Only in the case of low subcarrier numbers, do we need to improve the SIR by adding CP.

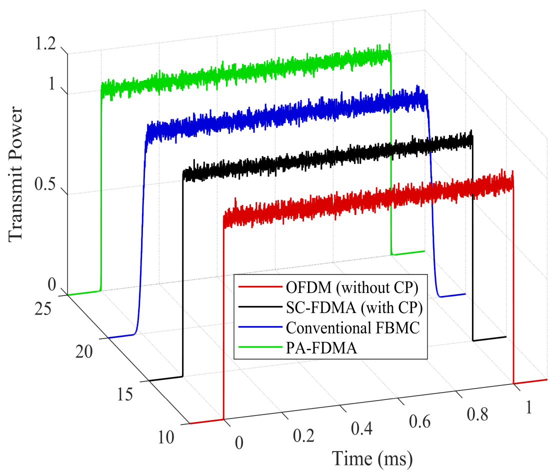

Fig. 2. Transmitted power for different systems. To avoid overlaps that lead to an inability to distinguish the different systems' powers, we plot them in a 3D view. We can observe that PA-FDMA has almost the same transmitted power as SC-FDMA.

A. PAPR

Fig. 2 shows the transmitted power of the different systems. The signal power values are different at various moments, but the average power is 1. We observe that SC-FDMA has lower peak power compared to OFDM. The same conclusion can be observed between PA-FDMA and FBMC. To analyse the relationship between peak power and mean power more explicitly, we adopt PAPR for evaluation. For a fair comparison with OFDM etc., we calculate the PAPR over one symbol time spacing, denoted as

$$\mathrm{PAPR} = \frac{\max\limits_{kT<t<(k+1)T}\left(|s(t)|^2\right)}{\mathrm{E}\left\{|s(t)|^2\right\}},\ k = 1, 2, \cdots, K \tag{22}$$

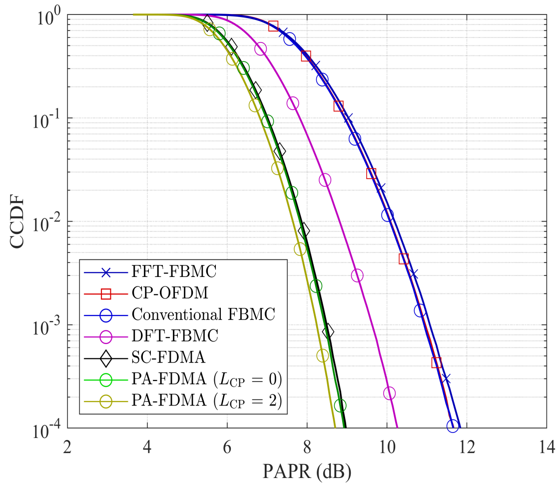

Fig. 3. CCDF of PAPR for different systems. PA-FDMA features almost the same PAPR as SC-FDMA. The addition of CP is equivalent to eliminating the base pulse, so the PAPR is enhanced.

Then, we adopt the Complementary Cumulative Distribution Function (CCDF) for evaluation. We take the subcarrier number $L = 128$ and the modulation order 16-QAM. Fig. 3 shows the CCDF of PAPR for different systems.

Conventional FBMC has poor PAPR like OFDM. However, PA-FDMA features nearly the same PAPR as SC-FDMA. FFT-FBMC [10] has the worst PAPR and thus is not considered subsequently.

B. BER over different channels

For numerical evaluation, we consider the below parameter configurations: The channel models we adopt are 3GPP 38.900

TABLE I
SIMULATION PARAMETERS

Parameter names	**Value**
Carrier frequency	2.5GHz
Frequency spacing	$F = 15$kHz
Subcarrier number	$L = 128$
Symbol number	$K_{OFDM} = 14$, $K_{FBMC} = 15$
Sampling rate	$f_s = 5.04$MHz
Modulation order	16-QAM

"Pedestrian A" and "Vehicular A". We configure different mobility velocities for different scenarios and emulate multipath transmission by increasing the Wide-sense Stationary Uncorrelated Scattering (WSSUS) number.

For the flat channel, we set the velocity to 3km/h and the WSSUS number to 50 for the "Pedestrian A" channel model. Fig. 4 shows the BER curves with different systems for a flat channel.

Over a flat fading channel, all systems have almost the same BER performance. However, slight differences exist among the different systems, which can be explained by channel-induced interference. Although the channel environment matches low velocity and small multipath numbers, such nearly flat channels induce a few interferences.

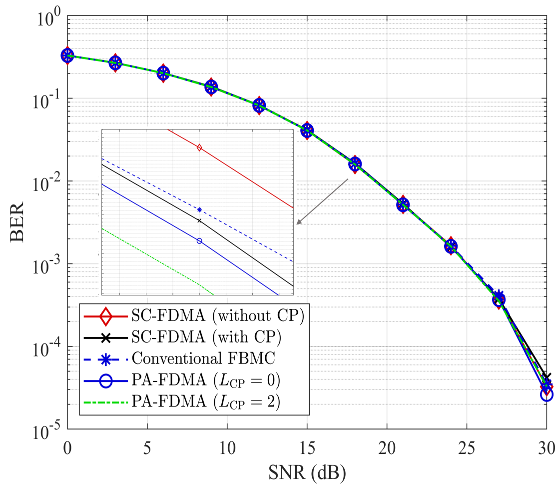

Fig. 4. BER performance over flat fading channel. All systems feature nearly the same BER performance. The slight variations observed among different systems primarily stem from interference induced by the channel.

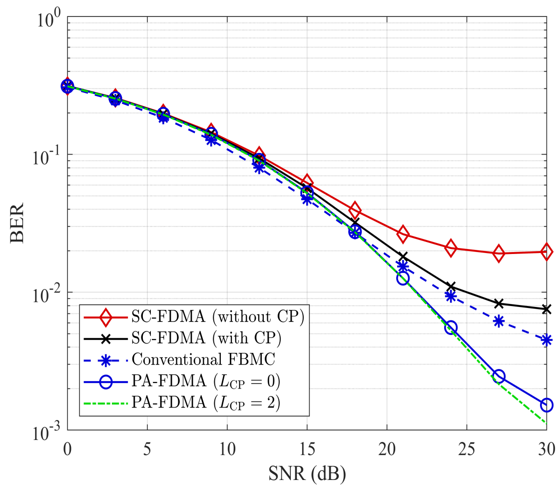

Fig. 5. BER performance over doubly selective channel. When the velocity is 350km/h, SC-FDMA suffers from serious inter-subcarrier interference. Thus, it has poor BER performance.

For the doubly selective channel, we set the velocity to 350km/h and the WSSUS number to 200 for the ”Vehicular A” channel model. Fig. 5 shows the BER curves for different systems with doubly selected channel. We consider SC-FDMA without CP because it features the same transmission rate as PA-FDMA. This allows us to make a fair comparison. Note that we take the CP time spacing of SC-FDMA to be $T_{CP} = 4.76\mu$s. Overall, SC-FDMA suffers from subcarrier interference and has poor BER performance. However, our scheme not only performs well in flat channels but also works robustly in doubly selective channels.

V. Conclusion

The proposed PA-FDMA is superior to SC-FDMA in many areas. For example, PA-FDMA can work robustly in doubly selective channels without CP and features lower PAPR and OOB emission. Additionally, PA-FDMA can eliminate the imaginary interference of FBMC and exhibit OFDM-like complex orthogonality transmission. Potential applications of PA-FDMA include uplink transmission for wireless communications as well as machine-type communications. Its good time-frequency properties ensure that no strict synchronization license is required among different users. However, the slightly higher delay sensitivity of PA-FBMC poses a challenge for real-time communication applications. Thus, the integration of low-latency transmission techniques to improve the real-time performance of the system becomes an important focus for future research.

References

[1] P. Schulz et al., ”Latency critical IoT applications in 5G: Perspective on the design of radio interface and network architecture,” IEEE Communications Magazine, vol. 55, no. 2, pp. 70-78, 2017.

[2] H. Hosseiny, A. Farhang, and B. Farhang-Boroujeny, ”Downlink precoding for FBMC-based massive MIMO with imperfect channel reciprocity,” in ICC 2022-IEEE International Conference on Communications, 2022: IEEE, pp. 1324-1329.

[3] Y. Wang, Q. Guo, J. Xiang, L. Wang, and Y. Liu, ”Bi-orthogonality recovery and MIMO transmission for FBMC Systems based on non-sinusoidal orthogonal transformation,” Signal Processing, p. 109427, 2024.

[4] B. Farhang-Boroujeny, ”OFDM versus filter bank multicarrier,” IEEE signal processing magazine, vol. 28, no. 3, pp. 92-112, 2011.

[5] R. Nissel, S. Schwarz, and M. Rupp, ”Filter bank multicarrier modulation schemes for future mobile communications,” IEEE Journal on Selected Areas in Communications, vol. 35, no. 8, pp. 1768-1782, 2017.

[6] Y. Qi, J. Dang, Z. Zhang, L.Wu, and Y.Wu, “Efficient channel equalization and performance analysis for up link FBMC/OQAM-based massive MIMO systems,” IEEE Trans. Veh. Technol., vol. 72, no. 9, pp. 1–16, Sep. 2023.

[7] H. G. Feichtinger and T. Strohmer, Gabor analysis and algorithms: Theory and applications. Springer Science & Business Media, 2012.

[8] Y. Wang, Q. Guo, J. Xiang, and Y. Liu, ”Doubly selective channel estimation and equalization based on ICI/ISI mitigation for OQAM-FBMC systems,” Physical Communication, p. 102120, 2023.

[9] C. Lélé, P. Siohan, and R. Legouable, ”The alamouti scheme with CDMA-OFDM/OQAM,” EURASIP Journal on Advances in Signal Processing, vol. 2010, pp. 1-13, 2010.

[10] R. Zakaria and D. Le Ruyet, ”A novel filter-bank multicarrier scheme to mitigate the intrinsic interference: Application to MIMO systems,” IEEE Transactions on Wireless Communications, vol. 11, no. 3, pp. 1112-1123, 2012.

[11] R. Nissel, J. Blumenstein, and M. Rupp, ”Block frequency spreading: A method for low-complexity MIMO in FBMC-OQAM,” in 2017 IEEE 18th International Workshop on Signal Processing Advances in Wireless Communications (SPAWC), 2017: IEEE, pp. 1-5.

[12] R. Nissel and M. Rupp, ”Enabling low-complexity MIMO in FBMC-OQAM,” in 2016 IEEE Globecom Workshops (GC Wkshps), 2016: IEEE, pp. 1-6.

[13] R. Nissel and M. Rupp, ”Pruned DFT-spread FBMC: Low PAPR, low latency, high spectral efficiency,” IEEE Transactions on Communications, vol. 66, no. 10, pp. 4811-4825, 2018.

[14] T. Ihalainen, A. Viholainen, T. H. Stitz, M. Renfors, and M. Bellanger, ”Filter bank based multi-mode multiple access scheme for wireless uplink,” in 2009 17th European Signal Processing Conference, 2009: IEEE, pp. 1354-1358.

[15] D. Na and K. Choi, ”Low papr fbmc,” IEEE Transactions on Wireless Communications, vol. 17, no. 1, pp. 182-193, 2017.

[16] R. W. Bauml and R. F. H. Fischer, ”Reducing the peak-to-average power ratio of multicarrier modulation by selected mapping,” Electronics Letters, vol. 32, no. 22, pp. 2056-2057, 1996.

[17] S. H. Muller and J. B. Huber, ”OFDM with reduced peak-to-average power ratio by optimum combination of partial transmit sequences,” Electronics Letters, vol. 33, no. 5, pp. 368-369, 1997.

[18] H. G. Myung, J. Lim, and D. J. Goodman, ”Single carrier FDMA for uplink wireless transmission,” IEEE vehicular technology magazine, vol. 1, no. 3, pp. 30-38, 2006.

[19] S. Sesia, I. Toufik, and M. Baker, LTE-the UMTS long term evolution: from theory to practice. John Wiley & Sons, 2011.

[20] M. Bellanger et al., ”FBMC physical layer: a primer,” PHYDYAS, January, vol. 25, no. 4, pp. 7-10, 2010.

[21] Q. Guo, Y. Wang, J. Xiang, and Y. Zhong. Complex Gaussian Ratio-Based Bit Error Probability Calculation for PAM-FBMC Systems. IEEE Communications Letters, 28(4):788–792, 2024.

[22] G. Berardinelli, K. I. Pedersen, T. B. Sorensen, and P. Mogensen, ”Generalized DFT-spread-OFDM as 5G waveform,” IEEE Communications Magazine, vol. 54, no. 11, pp. 99-105, 2016.

[23] G. Berardinelli, F. M. Tavares, T. B. Sørensen, P. Mogensen, and K. Pajukoski, ”Zero-tail DFT-spread-OFDM signals,” in 2013 IEEE Globecom Workshops (GC Wkshps), 2013: IEEE, pp. 229-234.

[24] A. Dutt and V. Rokhlin, ”Fast Fourier transforms for nonequispaced data,” SIAM Journal on Scientific computing, vol. 14, no. 6, pp. 1368-1393, 1993.

[25] S. F. Potter, N. A. Gumerov, and R. Duraiswami, ”Fast interpolation of bandlimited functions,” in 2017 IEEE International Conference on Acoustics, Speech and Signal Processing (ICASSP), 2017: IEEE, pp. 4516-4520.